Title

Correlating dilute solvent interactions to morphology and OPV device performance

Journal

Organic Electronics, 14(10)

ISSN

1566-1199

Authors

Chang, Lilian
Jacobs, Ian E
Augustine, Matthew P
et al.

Publication Date

2013-10-01

DOI

10.1016/j.orgel.2013.06.016

Peer reviewed

Organic Electronics 14 (2013) 2431–2443

Contents lists available at SciVerse ScienceDirect

Organic Electronics

journal homepage: www.elsevier.com/locate/orgel

Correlating dilute solvent interactions to morphology and OPV device performance

Lilian Chang [a], Ian E. Jacobs [a], Matthew P. Augustine [b], Adam J. Moulé [a,*]

[a] Department of Chemical Engineering and Materials Science, University of California, Davis, One Shields Avenue, CA 95616, USA
[b] Department of Chemistry, University of California, Davis, USA

ARTICLE INFO

Article history:
Received 10 April 2013
Received in revised form 18 June 2013
Accepted 18 June 2013
Available online 1 July 2013

Keywords:
Bulk-heterojunction
Organic photovoltaic
Solvent additive
Morphology
Cross-link
Device longevity

ABSTRACT

Solvent additives have been explored as a reliable way to control the morphology in bulk-heterojunction (BHJ) layers for improved device performance. We show that the choice of solvent additives has direct implications on morphological evolution, i.e. poly(3-hexylthiophene) (P3HT): [6,6]-phenyl C61-butyric acid methyl ester (PCBM) BHJ films processed with a small amount of 1,8-diiodooctane or 1-chloronaphthalene have more crystalline PCBM domains compared to crystalline P3HT domains, while the opposite is true for films cast with nitrobenzene additive and films cast purely from chlorobenzene. The BHJ film cross-links when annealed at 300 °C in the presence of 1,8-diiodooctane. Cross-linking is found to occur even in pristine P3HT and PCBM films annealed under similar conditions. NMR spectroscopy is presented as a viable technique for quantitative analysis of the amount of solvents left in the BHJ films before and after heat treatment. Despite differences in the ways the additives affect the morphology of the BHJ layer, device performance remained stable over 300 h for all additives tested.

1. Introduction

Organic photovoltaic (OPV) devices have the potential to be unparalleled in terms of processing cost, scalability, speed, and simplicity. The simplest of such devices consists of a single bulk-heterojunction (BHJ) active layer, in which the electron donor (typically a conjugated polymer) and electron acceptor (typically a fullerene) are deposited from a common solvent. The electron donor and electron acceptor phase-separate during solvent evaporation, yielding a nanoscale interpenetrated network with donor–acceptor heterojunctions throughout the photoactive layer [1,2]. BHJ films are typically deposited via spin-coating, which results in a morphology that is quenched into a non-equilibrated state. Recent study of poly (3-hexylthiophene) (P3HT): [6,6]-phenyl C61-butyric acid methyl ester (PCBM) BHJ layer formation using time-resolved spectral reflectometry (TRSR) together with grazing incidence small and wide angle X-ray scattering (GIWAXS/GISAXS) revealed that the BHJ solution thins rapidly following a non-linear behavior during spin-coating and P3HT crystallization and phase separation occur rapidly and simultaneously [3]. At P3HT to PCBM ratio of 1:1, P3HT crystallization is initiated closer to the end of the drying process, forming a glassy solid solution [3]. Hence, a controlled thermal annealing step has been widely used post BHJ layer deposition to "improve" the morphology of the BHJ layer, allowing the donor and acceptor to reorganized into a lower energy conformation [4–7]. However, extensive phase-separation can lead to the formation of pure domains that are larger than the exciton diffusion length [8], preventing excitons from diffusing to a donor–acceptor interface for charge separation [9]. This indicates that there is an optimal phase-separated morphology for maximum power conversion efficiency [6]. Of equal concern is the thermal stability of the BHJ morphology.

* Corresponding author. Address: Department of Chemical Engineering and Materials Science, 3001 Ghausi Hall, One Shields Avenue, University of California, Davis, CA 95616, USA. Tel.: +1 530 754 8669; fax: +1 530 752 1031.
E-mail address: amoule@ucdavis.edu (A.J. Moulé).

1566-1199/$ - see front matter © 2013 Elsevier B.V. All rights reserved.
http://dx.doi.org/10.1016/j.orgel.2013.06.016

The best morphology for superior device performance will in all likelihood not be at its most thermodynamically stable state, leading to a coarsening of domains over time especially at elevated temperatures. Typical rooftop temperatures can range from −20 °C on a cold night, to a high of 80 °C, which is hot enough to induce some morphological changes in the BHJ layer. It is therefore of tantamount importance that the BHJ morphology be robust against morphology changes at operating temperatures. The realization of the importance of lifetime studies on OPV devices has led to efforts in standardizing reports on stability and lifetime data to allow for better comparison across laboratories [10].

BHJ morphology control has been intensely researched [11,12]. The desire for morphology control has led to the exploration of new materials (for example, cross-linkable materials [13] and block-copolymers [14–16]), and the rise of various processing techniques (thermal and solvent annealing [4,17,18], solvent additives [19–23], and changing parameters such as solvent, polymer:fullerene ratio, and solution concentration [24–26]). The importance of solvent in the BHJ morphology has been long established [11,5,27]. In an effort to achieve the optimal morphology for superior device performance, researchers have explored various ways to influence the property of the solvents used in BHJ layer processing, including the use of solvent additives [19–23,28]. Efforts were also invested in the understanding of morphological evolution and recently, several studies alluded to the partial miscibility of fullerene derivatives in polymer matrices [29–33]. The studies suggest that amorphous polymer chains are miscible with amorphous fullerene in the mixed domains, leading to the conclusion that at least three phases are present in the P3HT:PCBM BHJ layers, i.e. pure P3HT phase, PCBM-rich phase, and mixed P3HT–PCBM phase [32].

The use of co-solvents for BHJ solar cells was first introduced by Zhang et al. [19]. Following this work, various solvent additives, e.g. alkanethiols [20,28], 1-chloronaphthalene (CN) [23], 1,8-diiodooctane (DIO) [22], and nitrobenzene (NB) [21], have been explored. These additives affect P3HT and PCBM phase-separation mechanism differently in BHJ films [34]. While there has been rationalization on the mechanism by which the processing additives control morphology [35,22,21], much ambiguity still surrounds the exact mode of interaction between these additives and the polymer–fullerene component in the BHJ layer. Since some of the additives used are reactive, we question whether there are any peripheral effects beyond the phase-separation mechanism, and if there are any consequences on the longevity of the OPV devices.

We have previously reported that trace solvents, especially "good" solvents for P3HT, can be retained within the BHJ film, causing significant changes in morphology development when the film is subjected to heat treatment [36]. This is corroborated by research that showed that solvent removal from polymeric thin films is not trivial [37,38]. This article explores how the initial morphology of the P3HT:PCBM BHJ layer can be controlled through the use of solvent additives, how these impurities affect the thermal stability of the BHJ morphology, and device performance over time. We present a feasible way to quantify the amount of trace solvents left in the P3HT:PCBM BHJ film using nuclear magnetic resonance (NMR) spectroscopy. While we do not claim to have a complete understanding of the complex solvent-polymer-fullerene interactions, our work detailed in this paper elucidates some interesting insights into the morphology of BHJ layer processed with solvent additives. It has been established that some solvents affect the fullerene phase more than the polymer phase [22,39]. We show proof that the crystalline content within each phase can differ depending on the additives used. We also uncover a thermally activated reaction that causes cross-linking in pristine P3HT and PCBM films and also in the blended BHJ films, in the presence of DIO. Despite differences in the morphology of the BHJ layer processed using different solvent additives, it is interesting that device performance remained stable over at least 300 h for all additives tested.

2. Results and discussion

2.1. Solvent additives

Three solvent additives, i.e. NB, DIO, and CN, were investigated in this paper based on the premise that they interact differently with the P3HT and PCBM components within the BHJ layer. All three additives have boiling points higher than the host solvent, chlorobenzene (CB). NB is a polar "non-solvent" for P3HT and also a "poor" solvent for PCBM. The addition of NB to the casting solvent increases aggregation and order within the P3HT domains [21]. DIO is selectively a better solvent for PCBM [22], allowing PCBM to remain in solution longer to avoid excessive PCBM aggregation in the BHJ layer [39]. CN is a "good" solvent for both P3HT and PCBM. The slower evaporation rate during spin-coating allows a longer time for P3HT chains to self-organize into highly ordered molecular structure for higher hole mobility [23]. Our group has previously shown that the P3HT:PCBM BHJ active layer has high affinity towards solvent molecules and that solvents can remain trapped within the layer, increasing the diffusive mobility of PCBM within the P3HT matrix and promoting the growth of larger PCBM agglomerates [36].

The choice of solvent additive has been shown to affect domain sizes and hence surface roughness of the BHJ film [22,40]. Fig. 1 shows root mean square (RMS) roughness of films processed from chlorobenzene (CB) alone and with 4 vol.% of NB, DIO, and CN, as-cast and after heat treatment at various temperatures. These RMS values were obtained from atomic force microscopy (AFM) topography images collected over a scan size of 5 μm by 5 μm. It is observed that CB-cast films remained relatively smooth (RMS roughness below 1.1 nm) regardless of heat treatment temperature. As-cast, P3HT:PCBM films from CB are largely amorphous [7] and a skin of P3HT has been shown to form at the air interface during spin-coating [41,42], resulting in a relatively smooth film. While annealing enhances ordering of the P3HT phase, the amorphous P3HT-rich skin has been shown to persist after heat treatment [42], which is likely why the films remained flat. Films that result from solutions with 4 vol.% additives exhibited higher surface

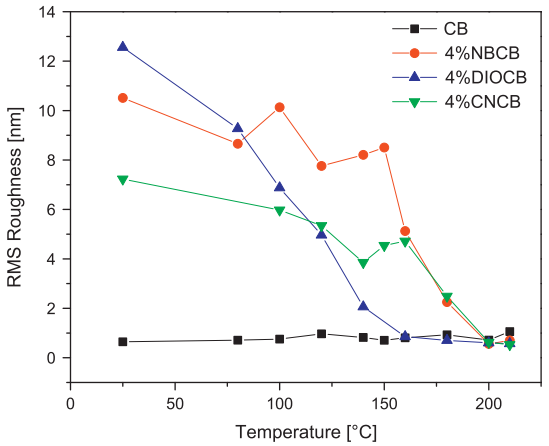

Fig. 1. RMS roughness from AFM topography images of P3HT:PCBM (1:1) films, collected over a range of treatment temperature.

roughness as-cast. This is because these films were already substantially phase-separated after spin-coating and a higher volume of the film are crystalline compared to CB-cast films. The films become smoother when annealed, likely due to surface energy effects causing vertical segregation of components within the BHJ layer. It has been shown that there is an enrichment of PCBM under the P3HT skin after heat treatment [43,42] and that the presence of solvent additives affects the vertical segregation profile, i.e. the concentration of PCBM at the interface is lower in NB/CB BHJ films compared to CB films [42].

NB/CB films seem to remain rougher over a larger range of annealing temperatures compared to DIO/CB films likely because of the formation of an aggregated P3HT network within the film [21] and the lower concentration of PCBM in the PCBM-enriched region near the air interface after heat treatment [42]. This is consistent with our previous results showing the formation of ordered P3HT domains in NB/CB films at higher temperatures compared to CB-cast films [36]. RMS surface roughness for the DIO/CB film decreases immediately when subjected to heat, while the decrease in RMS roughness for CN/CB film is more gradual. The surface roughness decreases drastically for NB/CB and CN/CB films when heat-treated beyond 150 °C. The change in RMS surface roughness with applied heat indicates that thermal input necessarily causes morphological changes. Notably, despite differences between the RMS surface roughness of solvent-additive-processed layers with CB-cast samples, devices from as-cast NB/CB, DIO/CB, and CN/CB devices have been shown to have similar if not superior performance to annealed CB-cast samples [21–23].

Table 1
Amount of additives in BHJ films as-cast and after heat treatment at 150 °C for 5 min, calculated mass % relative to total film mass from data shown in Fig. 2.

BHJ film	As-cast/mass (%)	Heat-treated mass (%)
NB/CB	0.5	0.04
DIO/CB	70.0	0.01
CN/CB	1.0	0.05

Table 1 shows the calculated amount of solvent additives left in as-cast and heat-treated BHJ films based on the NMR spectra shown in Fig. 2. The signals for PCBM are used as a reference to calculate the mass % of solvent in the P3HT:PCBM (1:1) BHJ film. All three additives were significantly removed from the BHJ film after heat treatment at 150 °C for 5 min in a N_2 glovebox. The results reveal that the amount of DIO present in as-cast DIO/CB sample is significantly more than the amount of PCBM in the film, i.e. 70 mass % relative to total film mass. The substantial presence of DIO in as-cast BHJ films probably increases the diffusion of PCBM into the enrichment zone near the sample-air interface during heat treatment, hence the drastic decrease in RMS roughness for the DIO/CB sample when heat is applied. In contrast to DIO, NB and CN are only present in very small amounts in as-cast films. While we have previously used GCMS to detect the presence of trace solvents in BHJ films qualitatively [36], we can now quantify the amount of solvents left in the film using NMR.

In order to investigate the effect of solvent additives on the BHJ layer, thermal analysis was performed on films cast from CB and various solvent additives using differential scanning calorimetry (DSC). Fig. 3 shows DSC thermograms recorded during heating of P3HT:PCBM (1:1) films processed with CB and with 4% solvent additives. Samples were cast onto glass substrates, delaminated, and subse-

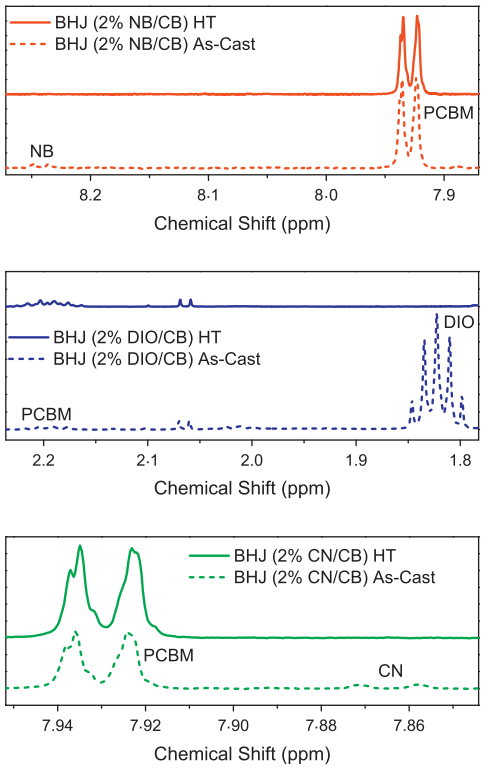

Fig. 2. 1H NMR spectra for 2% NB/CB, 2% DIO/CB, and 2% CN/CB, as-cast (dashed lines) and after heat treatment at 150 °C for 5 min in a nitrogen glove box equipped with a molecular sieve solvent trap and is under continuous gas flow. Each of the PCBM signals and the NB signal originates from two protons, while the DIO signal originates from four protons and the CN signal originates from a single proton.

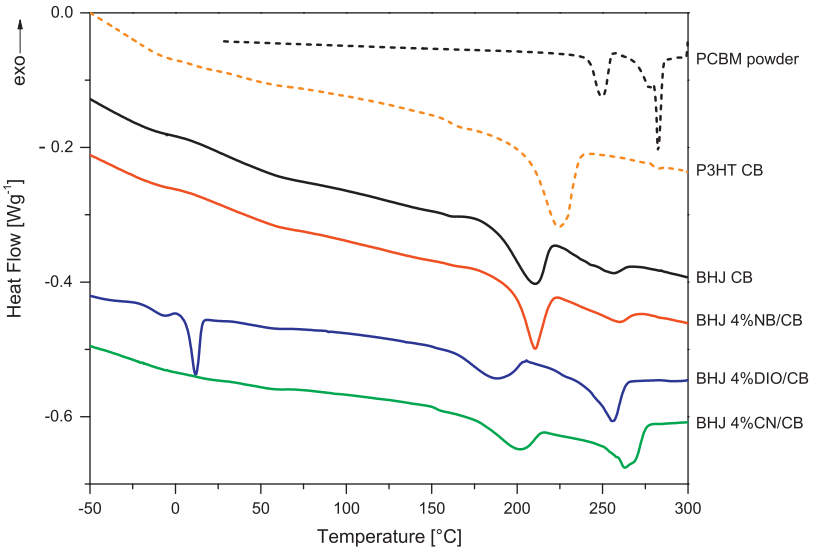

Fig. 3. DSC heating traces of P3HT:PCBM (1:1) with isothermal step at 150 °C for 30 min. Thermograms are shifted vertically for clarity.

quently loaded into aluminum crucibles with pierced lids. Heating curves for a pristine P3HT film cast from CB and powder PCBM are shown for reference. Powder PCBM was used due to difficulty in obtaining the required sample weight for a CB-cast film. The heating curves were recorded after an isothermal step at 150 °C for 30 min to emulate the typical heat treatment step during device fabrication [5].

The phase transition observed at approximately 50 °C in the films have been attributed to the melting of the P3HT side-chain [44]. The feature at 12 °C for the 4% DIO/CB film is due to the melting of DIO. We have previously shown that trace solvent can be trapped in the films [36], and since the samples were "annealed" at 150 °C in a sealed crucible with a tiny perforation on the lid in the DSC chamber, it is plausible that some solvent remained within the sample. It is also likely that most of the trapped DIO evaporates during the heating routine. Pristine CB-cast P3HT film has a melting temperature (T_m) of *ca.* 224 °C. A well-defined melting endotherm is indicative of the presence of crystalline domains of either P3HT or PCBM phases. Previous studies have shown the likelihood of at least 3 phases in the BHJ film [30,32]. A pure P3HT phase is likely present in the BHJ film since fullerenes cannot intercalate into the crystalline domains of P3HT [45,46]. The mixed phase consists of amorphous P3HT with amorphous PCBM, while the fullerene-rich phase consists of PCBM and amorphous P3HT [32]. $T_{m,P3HT}$ in CB and 4% NB/CB BHJ films is approximately 14 °C lower, at *ca.* 210 °C. The depression of $T_{m,P3HT}$ in the presence of PCBM has been previously reported [47], implying some degree of miscibility between P3HT and PCBM [48,30]. Interestingly, the heating curves for CB and 4% NB/CB films look similar, contrary to what we previously reported [36]. This is likely due to sample preparation and history, e.g. small variation in the amounts of trace solvent trapped within the film prior to the DSC scans. We have since improved and standardized the sample preparation procedure, especially when dealing with solvents of various boiling points. The endotherm at *ca.* 255 °C for the CB BHJ sample corresponds to the melting of PCBM (*ca.* 259 °C for the NB/CB film). $T_{m,P3HT}$ is considerably lowered in 4% DIO/CB and 4% CN/CB samples, *ca.* 186 °C and *ca.* 200 °C respectively, i.e. $T_{m,P3HT}$ occurs at higher temperatures for CB and NB/CB films compared to DIO/CB and CN/CB films. Further depression of $T_{m,P3HT}$ in DIO/CB and CN/CB films indicate differences in the Flory–Huggins interaction parameter and the miscibility of amorphous P3HT:PCBM mixtures. The enthalpy of fusion, $\triangle H_f$ (area under curve of the melting peaks), for P3HT and PCBM appear almost similar for CB and NB/CB samples, and for DIO/CB and CN/CB films, which suggests that there is a fundamental difference between CB and NB/CB films, and DIO/CB and CN/CB films. The $\triangle H_f$ and T_m extracted from Fig. 3 are summarized in Table 2.

Since $T_{m,P3HT}$ for CB and NB/CB samples are closer to the T_m for pristine P3HT, we can surmise that the P3HT crystals in these films approaches the behavior of P3HT crystals in a pristine P3HT film. The higher $T_{m,P3HT}$ and steeper P3HT melting endotherms for CB and NB/CB samples suggest that the amount of ordered P3HT domains are larger in

Table 2
Melting peak and enthalpy of melting (approximate from area under melting peak) for P3HT and PCBM from Fig. 3.

Sample	$T_{m,P3HT}$ (°C)	$\triangle H_{m,P3HT}$ (J g^{-1})	$T_{m,PCBM}$ (°C)	$\triangle H_{m,PCBM}$ (J g^{-1})
PCBM	-	-	250, 282	8.99
P3HT	224	18.8	-	-
BHJ CB	210	8.2	255	2.6
BHJ 4% NB/CB	210	7.2	259	2.7
BHJ 4% DIO/CB	186	5.2	255	8.5
BHJ 4% CN/CB	200	5.2	263	7.9

these samples compared to the DIO/CB and CN/CB samples. The broad and shallow melting peaks for PCBM in CB and NB/CB films suggest a larger size distribution of PCBM crystals and smaller degree of crystallization in the PCBM phase. This is reasonable if P3HT ordering is the main driver of phase separation in heated CB and NB films, forcing PCBM into various crystal sizes. Our observation coincides with the conclusion presented by Gomez et al. They found that in samples prepared with CB, polymer crystallization drives the structure formation process in a typical 1:1 P3HT to PCBM blend [30]. During annealing, P3HT precipitates as a crystalline pure phase, forcing PCBM into the amorphous mixed phase. The concentration of PCBM increases in the mixed phase with increasing polymer crystallization, leading to macroscopic phase separation and the observation of micrometer-sized fullerene clusters [30]. In the case of the DIO/CB and CN/CB samples however, there is likely increased competition between P3HT and PCBM crystallization during heat treatment. Since DIO is a selectively better solvent for PCBM while CN is also a decent solvent for PCBM, PCBM remains in solution longer, allowing motion in the PCBM phase and providing sufficient time for PCBM to diffuse and aggregate together, resulting in a higher amount of crystalline PCBM within the film and hence a larger $\triangle H_{f,PCBM}$. This agrees with previous observation of larger PCBM crystals on the micrometer-scale in DIO/CB and CN/CB films compared to CB and NB/CB films [36]. As CB evaporates faster compared to DIO and CN, the solvent quality declines for P3HT, suppressing motion in the P3HT phase and forcing P3HT chains to aggregate into domains of various sizes (likely with defects), consequently yielding a broader and shallower melting endotherm (smaller $\triangle H_{f,P3HT}$). It is highly probable that film formation is driven by phase-separation and PCBM crystallization for DIO/CB and CN/CB films rather than P3HT crystallization as observed in CB and NB/CB films. Recent work by Durrant et al. [49] suggests that the tendency for PCBM to form crystalline domains is the reason behind its success as an electron acceptor material in OPV devices, although the authors note that PCBM crystallization is less of a factor when employed with P3HT, due to the latter's strong tendency to crystallize. This may explain the widespread success of DIO as an additive for various OPV devices employing $PC_{61}BM$ [40] and $PC_{70}BM$ [22,50,39], since blended films processed with DIO result in a higher amount of crystalline PCBM.

2.2. Heat-induced reaction

DSC heating traces for P3HT:PCBM BHJ film at a 1:4 ratio (PCBM-rich) with and without 4% solvent additives are shown in Fig. 4. This mixing ratio was selected to emphasize interactions between (amorphous) P3HT and PCBM while suppressing P3HT crystallization. In this experiment, the films were not isothermally treated, although sample preparation protocols were standardized as much as possible to minimize discrepancy in the thermal history of the samples. First heating and second heating curves were collected. The second heating curves were collected after the samples were quenched from 300 °C to −100 °C in the DSC. Cold crystallization exotherms for PCBM [47,51] are evident in both the first and second heating curves for CB, NB/CB, and CN/CB samples, while it is only seen in the first heating curve for the DIO/CB sample. In the first heating traces, cold crystallization peaks were observed at *ca.* 161 °C for the CB sample, *ca.* 135 °C for the NB/CB sample, *ca.* 134 °C for the DIO/CB sample, and *ca.* 130 °C for the CN/CB samples. In the second heating traces, cold crystallization peaks were observed between 167 °C and 168 °C for the CB, NB/CB, and CN/CB samples, while this feature was not detected in the DIO/CB sample. A small melting endotherm, attributed to the P3HT backbone, is seen at around 204 °C in the first heating curves for CB and NB/CB samples, and a broader melting endotherm is observed for CN/CB sample at *ca.* 214 °C. In the second heating traces, $T_{m,P3HT\ backbone}$ is between 207 °C and 209 °C for these 3

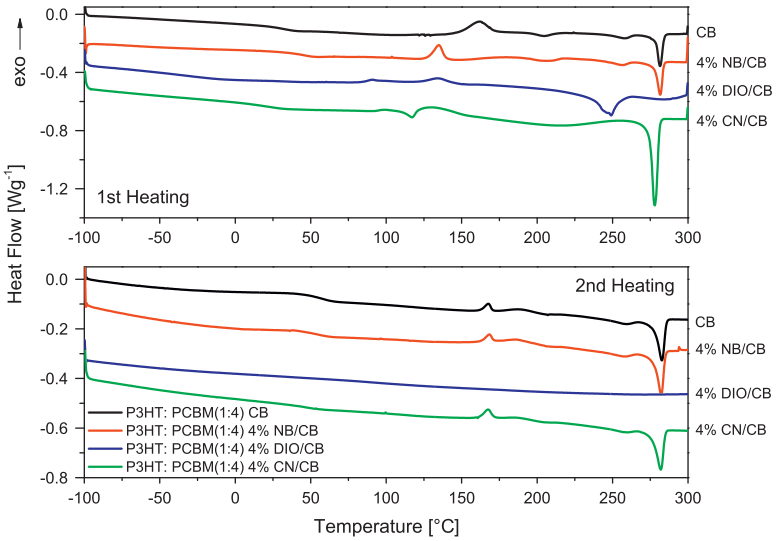

Fig. 4. DSC first (top) and second (bottom) heating traces for P3HT:PCBM (1:4) without isothermal step. Thermograms are shifted vertically for clarity.

samples. Evidently, the DIO/CB sample shows a completely different signature. While the melting endotherm for PCBM occurs at *ca.* 281 °C for both CB and NB/CB samples and *ca.* 278 °C for CN/CB samples, there is a significant depression in $T_{m,PCBM}$ in the DIO/CB sample (*ca.* 249 °C), and the melting endotherm of the P3HT backbone is not detected. In the second heating curve, the DSC thermogram for DIO/CB is almost featureless. This implies that after the first heating routine, crystallization of the P3HT and PCBM component is impeded during the quenching step and the subsequent second heating routine. Hence, we can conclude that heating the DIO/CB films up to 300 °C induces a change in the DIO/CB sample that prevents crystallization of P3HT and PCBM, at least in the 1:4 ratio shown.

Fig. 5 shows a comparison between P3HT:PCBM (1:4) films that were cast from CB (left) and 4% DIO/CB (right) using reflected optical microscope (ROM). The untreated (as-cast) films were quite featureless at the micrometer scale, while PCBM crystals [51] were observed in films that were heat-treated at 150 °C for 10 min. Consistent with previously reported results [36], PCBM crystals in the DIO/CB film appear larger in size and quantity, as shown in the higher magnification images in the inset of Fig. 5c and d. When the CB and DIO/CB films were subjected to heat treatment at 300 °C for 5 min, the size of the crystals increases. PCBM crystals in the DIO/CB sample (Fig. 5f) are significantly larger in comparison to the CB sample (Fig. 5e), likely due to increased PCBM diffusion rate in a DIO/CB film. An inspection of solvents left in BHJ films after

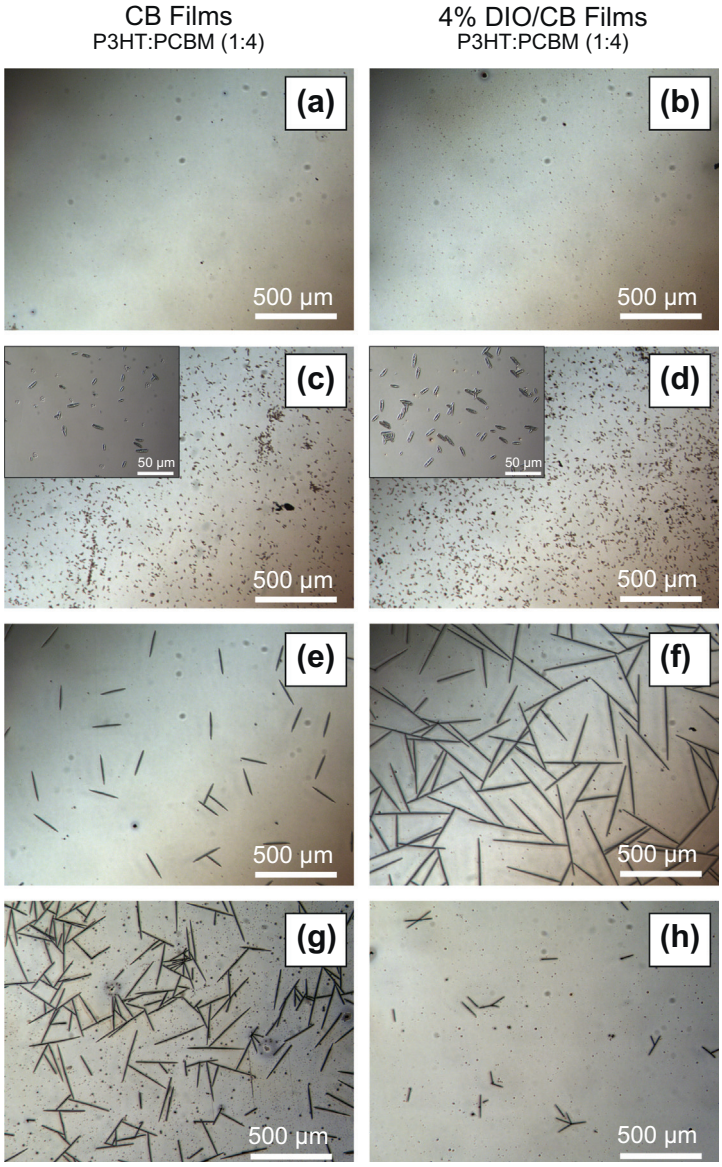

Fig. 5. Microscope images of P3HT:PCBM (1:4) films spin-coated from CB (left) and 4% DIO/CB (right): (a and b) as-cast, (c and d) after heat treatment at 150 °C for 10 min (inset shows higher magnification), (e and f) after heat treatment at 300 °C for 5 min, (g) after heat treatment at 300 °C for 5 min in CB-saturated environment, and (h) after heat treatment at 300 °C for 5 min in DIO-saturated environment.

heat treatment at 150 °C using NMR, revealed that most of the solvent additives were removed after 5 min when annealed in a nitrogen glove box equipped with a molecular sieve solvent trap (Fig. 2). So, the effect of the solvent additives on the rate of PCBM diffusion decreases with increasing heating time. When the films were heat-treated at 300 °C under solvent-saturated enviroment, i.e. the CB sample was annealed under CB-saturated environment, and the DIO/CB sample was annealed under DIO-saturated environment, the PCBM crystals in the CB sample increases in size and quantity (Fig. 5g) as expected due to an excess amount of solvent in the film resulting in a higher rate of PCBM diffusion into growing PCBM crystals during heat treatment. This logic would lead us to expect even larger PCBM crystals in DIO/CB films due to the higher boiling point of DIO and its preference for solvating PCBM over P3HT. Instead, the crystallization of PCBM in the DIO/CB sample is significantly suppressed (Fig. 5h). This observation corroborates the DSC results shown in Fig. 4. Since the DSC measurements were carried out in a sealed crucible with a tiny pierced hole on the lid, solvent vapors likely remained within the crucible during heating. Both the ROM images and the DSC results indicate a suppression in PCBM crystallization when a DIO/CB sample is heat-treated at 300 °C in the presence of DIO.

To test if the high-temperature induced changes seen in PCBM-rich samples extends to typical P3HT:PCBM ratios used in devices, P3HT:PCBM blends with 1:1 ratio were prepared from CB and DIO/CB solutions and studied using DSC. Fig. 6 shows DSC thermograms for P3HT:PCBM (1:1) cast from CB and from 4% DIO/CB samples. Both the first heating and second heating curves are shown. Similar to samples shown in Fig. 4, these films were not subjected to an isothermal step prior to measurements, hence the appearance of the cold-crystallization exotherm in the first heating curve. As previously mentioned, the endotherms observed at around 50 °C have been ascribed to the melting of P3HT side-chains [44]. The melting endotherm for P3HT backbone occurs at a lower temperature and appears to become broader and shallower upon the second heating in all cases. This is likely due to a decline in the degree of P3HT crystallinity (volume of crystalline P3HT domains within the film). The deep melting endotherm for PCBM seen in the first heating curve at *ca.* 258 °C is absent in the second heating curve for the DIO/CB sample, while a broad, shallow endotherm (for PCBM) is still present in the second heating curve for the CB sample. This implies that after the first heating routine, the DIO/CB sample is deficient in crystalline PCBM. This result reinforces the observations made in Fig. 4 and Fig. 5, despite the different P3HT to PCBM ratios. We have now established that the crystallization of PCBM is inhibited when P3HT:PCBM blend, either 1:4 ratio or 1:1 ratio, were heated to 300 °C in the presence of trace DIO. Similar signatures were observed when using a different source of P3HT (see Supplementary data Fig. S1).

P3HT:PCBM (1:1) BHJ films cast from CB and from all three additives were heat treated to 300 °C and examined using UV–vis spectroscopy as shown in Fig. 7a. For clarity, absorption spectra for the as-cast BHJ films are not shown on this figure but are shown in supplementary data, Fig. S2. The films were each heat-treated at 300 °C for 20 min, under saturated solvent environment depending on the casting solvent/solvent additive, i.e. the CB film was heat-treated under CB-saturated environment, the NB/CB film was heat-treated under NB-saturated environment, the DIO/CB film was heat-treated under DIO-saturated environment, and the CN/CB film was heat-treated under CN-saturated environment. After heat treatment, the samples were quenched to room temperature. Absorption spectra of the films were collected before and after washing the films with chloroform to detect if cross-linking has occurred. As shown in Fig. 7a, the absorption spectrum for the heat-treated DIO/CB film is vastly different compared

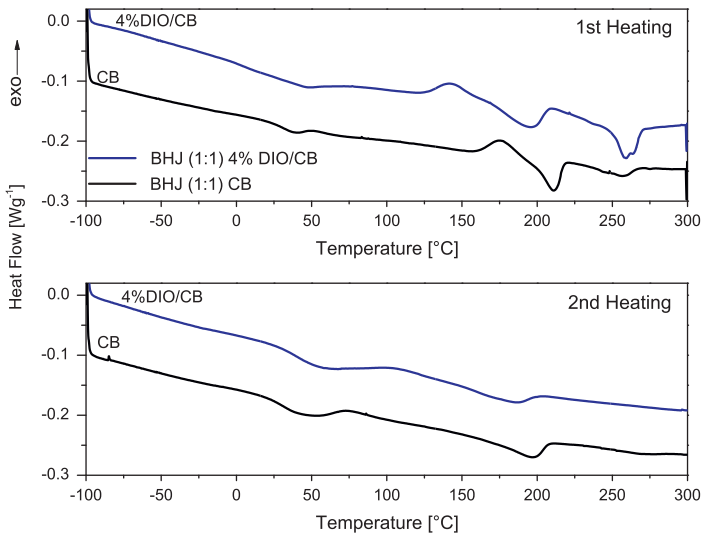

Fig. 6. DSC first (top) and second (bottom) heating traces for P3HT:PCBM (1:1) BHJ films without isothermal step. Thermograms are shifted vertically for clarity.

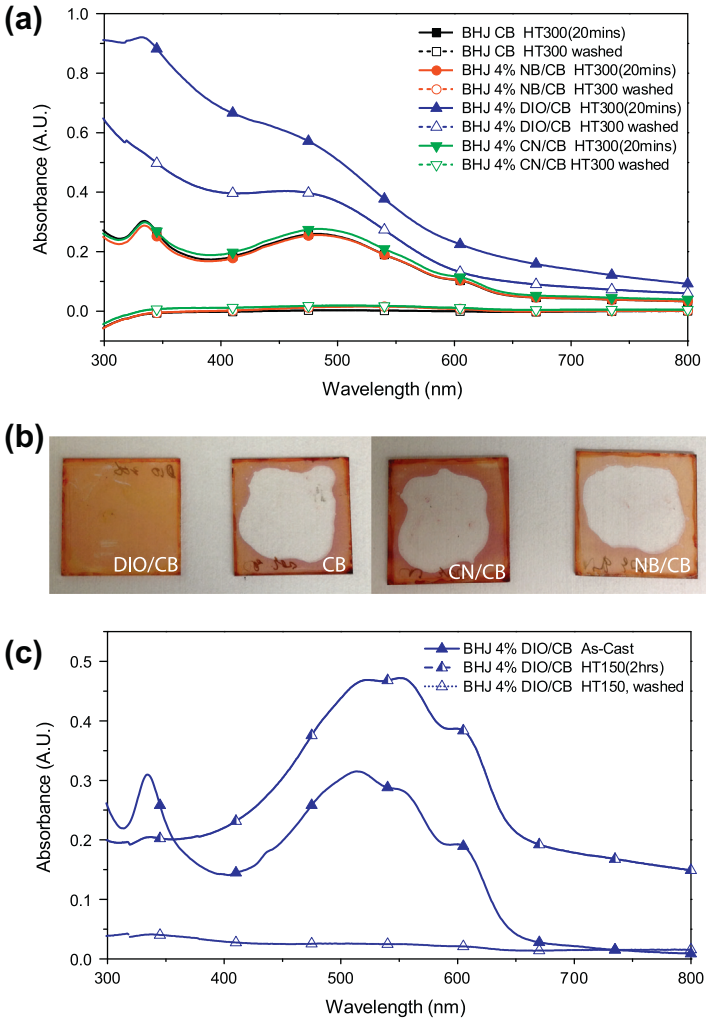

Fig. 7. (a) Absorption spectra of P3HT:PCBM (1:1) BHJ films cast from CB, 4% NB/CB, 4% DIO/CB, and 4% CN/CB after heat treatment at 300 °C for 20 min under solvent-saturated environment, and after chloroform wash. (b) Photo snapshots of samples in (a) after chloroform wash. (c) Absorption spectra of 4% DIO/CB (1:1) BHJ film as-cast, after heat treatment at 150 °C for 2 h under DIO-saturated environment, and after chloroform wash.

to the other films, with increased absorption in the blue. The absorption spectra of all the BHJ films post heat treatment at 300 °C suggest that the P3HT component within the blend is mostly amorphous due to the red-shifted absorption peak and the absence of distinct lower energy vibronic peaks. The CB, NB/CB and CN/CB films were removed after chloroform wash as evidence by the absence in absorption, shown in Fig. 7a, and photo snapshots of the washed films in Fig. 7b. Intriguingly, a seemingly complete film remained on the DIO/CB sample. Since DIO has been previously explored as a cross-linking agent [52], we postulate that the DIO/CB film has undergone cross-linking when subjected to heat treatment at 300 °C under DIO-saturated environment. When the DIO/CB films were subjected to 150 °C instead of 300 °C under similar DIO-saturated environment, it appears that the DIO/CB film was removed after chloroform wash despite prolonged duration of heat treatment (up to 2 h), as demonstrated in Fig. 7c. The increase in absorption below the bandgap after 2 h of heat treatment is likely caused by an increase in surface roughness. We can conclude that cross-linking is likely not an active mechanism during typical device fabrication conditions. However, knowledge of such reaction may become useful for future development of morphology control. There is also the possibility of manipulating reaction conditions so that a lower treatment temperature can be used once the mechanism of reaction becomes more known.

In order to isolate which component within the BHJ film is cross-linking, pristine films of P3HT and PCBM were fabricated and studied using UV–vis spectroscopy. Similar to samples in Fig. 7, the pristine samples were subjected to heat treatment at 300 °C for 20 min under solvent-saturated environment. Fig. 8 shows pristine P3HT film (Fig. 8a) and and pristine PCBM film (Fig. 8b), cast from CB and from 4% DIO/CB: as-cast, after heat treatment at 300 °C for 20 min, and after chloroform wash. It is clear that the chloroform wash removed both of the heat-trea-

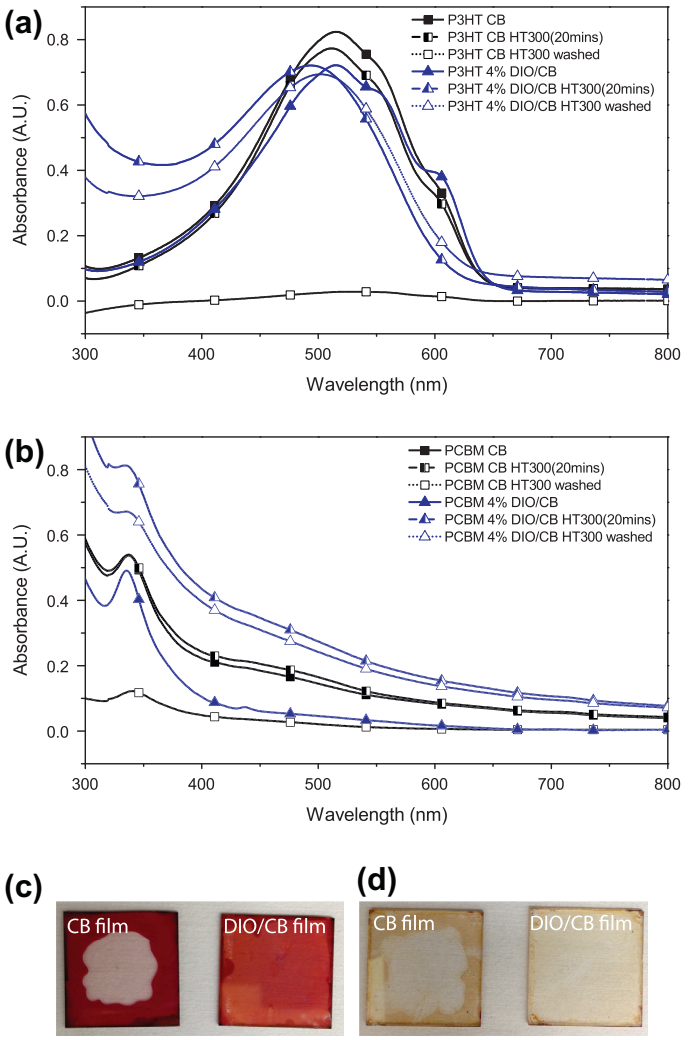

Fig. 8. Absorption spectra of (a) P3HT and (b) PCBM films cast from CB and 4% DIO/CB as-cast, after heat treatment at 300 °C for 20 min under solvent-saturated environment, and after chloroform wash. Photo snapshots of (c) P3HT and (d) PCBM films that were heat-treated at 300 °C for 20 min under solvent-saturated environment, before (left) and after (right) chloroform wash.

ted, CB-cast films for pristine P3HT and PCBM. The small absorption observed for CB-cast PCBM after chloforom wash is likely due to insufficient rinsing with chloroform. In the case of heat-treated DIO/CB films however, both pristine P3HT and pristine PCBM films appear intact after chloroform wash, evidenced by the absorption spectra and the photo snaphots for P3HT (Fig. 8c) and and PCBM (Fig. 8d) films. This leads to the deduction that both P3HT and PCBM undergo cross-linking with themselves and potentially with one another in a blended film when heated above 300 °C in the presence of DIO. This explains the absence of PCBM crystal melting endotherm and a decline in the degree of P3HT crystallinity in the DSC results. Cross-linked PCBM will not be able to diffuse to nucleation sites for crystal growth. Since P3HT is a polymer, it is likely that some of the polymer backbone can still π-stack to form crystalline domains despite the occurrence of cross-linking, leading to a reduction in the degree of crystallinity (broad and shallow melting endotherm) rather than a complete elimination of the melting endotherm. We postulate that the P3HT film is "loosely" cross-linked due to our observation that when chloroform was dropped onto the cross-linked P3HT film, the initially purple film turns orange. The chloroform that is then recollected from the film remained clear, while the film once again turns purple as the chloroform leaves the film. Analogous UV–vis experiments have been repeated with 2% DIO/CB with similar results (not shown) – an indication that the initial amount of DIO in the film has little effect as long as DIO is present during annealing at 300 °C.

2.3. Device performance over time

With the goal of investigating the implications of solvent additives on devices over time, we monitored the device performance of P3HT:PCBM (1:1) BHJ devices cast

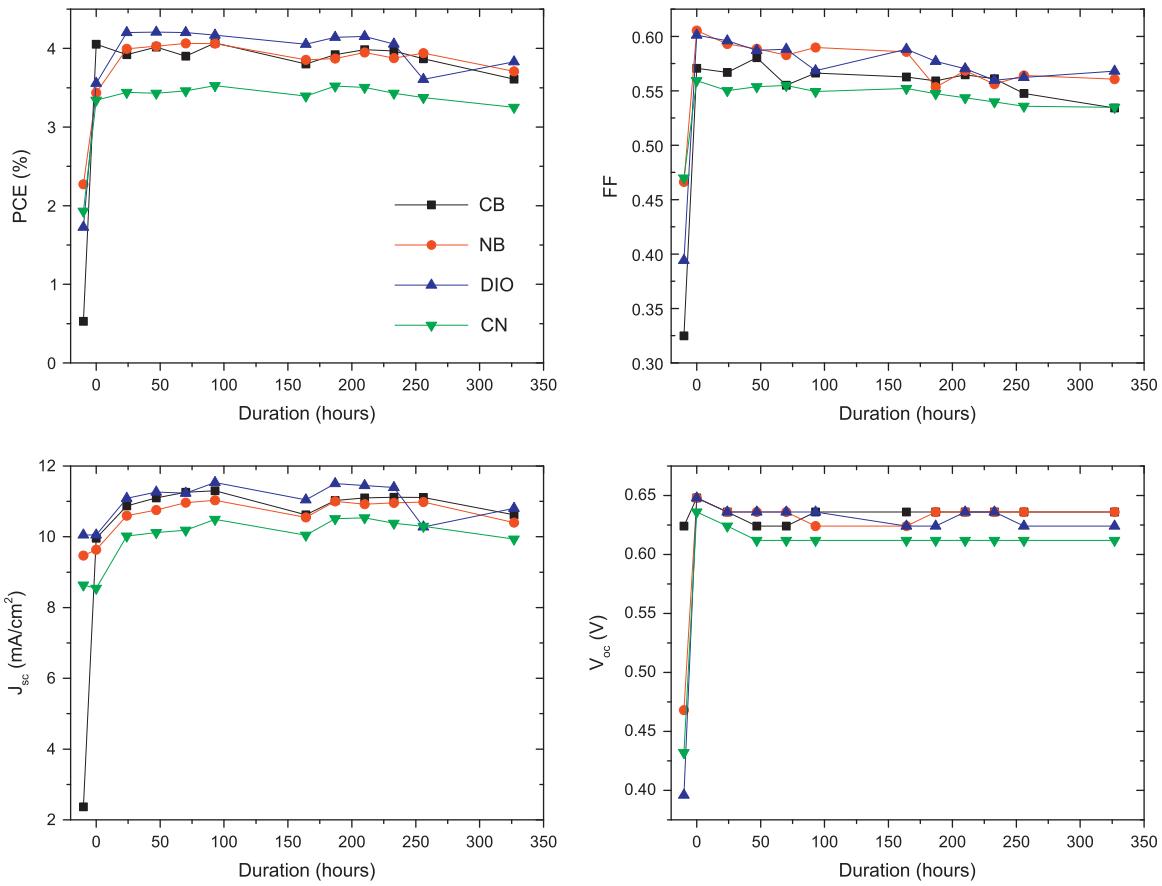

Fig. 9. Device performance monitored over a duration of 330 h for P3HT:PCBM (1:1) BHJ devices cast from CB, 4% NB/CB, 4% DIO/CB, and 4% CN/CB. Devices were stored at 80 °C in between test.

from CB, 4% NB/CB, 4% DIO/CB, and 4% CN/CB over a duration of 330 h, as shown in Fig. 9. Measurements were averaged over several devices and not from champion devices. In between tests, the devices were stored at 80 °C under open circuit conditions (i.e. disconnected from load). Devices were measured as-cast (data points before 0 h) and after an initial one-time heat treatment at 150 °C for 5 min (data points at 0 h). There appears to be a 24-h burn-in period, i.e. devices measured at 24 h showed an increase in short-circuit current density (J_{sc}), which in most cases resulted in a improvement in power conversion efficiency (PCE). CN/CB devices had the lowest PCE due to a lower fill factor (FF), J_{sc}, and open circuit voltage (V_{oc}), although the PCE remained fairly constant over 330 h with an overall drop of only *ca.* 0.19%. NB/CB and CB devices were almost comparable in device performance over time, except for the linear drop in FF for CB devices after 200 h. DIO/CB samples seem to perform the best over time, at least up to *ca.* 225 h. NB/CB, DIO/CB and CN/CB devices showed a slow decline in FF after approximately 150 h. Over the duration of 325 h, DIO/CB had the highest overall drop in PCE, *ca.* 0.37%, while CB and NB/CB devices dropped 0.31% and 0.29% respectively (after the burn-in period). Using NB and DIO as solvent additives appear to benefit the device over time, resulting in a stable FF, which may translate to a stable morphology. It is interesting that despite very different morphological evolution over temperature for NB/CB and DIO/CB films, as demonstrated by DSC, both afford efficient devices with stable performances spanning 330 h. Of course, in light of the discovery of the side-effects of DIO at higher temperatures, care has to be taken to ensure that we fully understand the role of solvent additives in the BHJ layer and the consequences of trace solvent within the film.

3. Conclusion

We have shown that the choice of solvent additives has direct implications on morphological evolution, favoring either a higher amount of crystalline P3HT domains or crystalline PCBM domains within the BHJ layer. DSC results show that DIO/CB and CN/CB BHJ (1:1) films post annealing at 150 °C, have more crystalline PCBM domains compared to crystalline P3HT domains, while the opposite is true in CB and NB/CB films. This implies that PCBM crystallization is favored over P3HT crystallization in DIO/CB and CN/CB BHJ films. When DIO is present during

heating at 300 °C, the BHJ film cross-links, as demonstrated by UV–vis absorption spectra after chloroform wash and the absence/decline of PCBM and P3HT crystalline content in the second heating curve on the DSC. Optical microscopy showed the formation of micrometer-sized PCBM crystallites in P3HT:PCBM (1:4) BHJ layers that were heat-treated at 300 °C in a nitrogen environment. However when DIO/CB films were heat treated at 300 °C under saturated DIO environment, a drastic suppression of PCBM crystallites was observed, substantiating the conclusion drawn from the DSC data. We have also shown that the cross-linking occurs even in pristine P3HT and PCBM films under similar conditions. It is likely that cross-linking between phases occurs as well in a blended film. Work is currently in progress to decipher the reaction mechanism behind the cross-linking behavior and the potential exploitation of this reaction for other interesting applications.

While we have previously established the presence of trace solvents in BHJ films using GCMS [36], NMR spectroscopy is a sensitive technique that can be used to quantify the amount of trace solvents in the BHJ films. The NMR results show significant amounts of DIO in as-cast P3HT:PCBM BHJ films as-cast, while most of the additives were removed after heat treatment at 150 °C for 5 min.

Remarkably, despite differences in the ways the additives affect the morphology of the BHJ layer, device performance did not discriminate the differences. Both NB/CB and DIO/CB devices offer high PCEs which remained stable over at least 300 h. This suggests that perhaps the crystalline content of each phase (after a certain threshold percentage) is no longer the major dictator of device performance. Since the function of the photoactive layer includes light absorption, exciton diffusion to the donor/acceptor interface, exciton dissociation at this interface, and transport of the resulting free charges through the two phases to the respective electrodes, it is possible that different solvent additives may primarily affect a different stage of the current generation process. It is also possible that the differences in crystalline content of the donor and acceptor phases have a lesser impact on P3HT:PCBM BHJ devices [49] compared to devices using other polymer-fullerene combinations.

In general, we expect that the P3HT becomes more insoluble with increasing molecular weights for all three additives tested in this paper while the solubility of PCBM remain unchanged. However, the longer polymer chains will likely take longer to relaxed, resulting in less crystalline P3HT domains under similar processing conditions. These two effects counteract each other. While the decrease in P3HT solubility encourages phase-separation, the decline in P3HT crystallinity leads to more mixed P3HT/PCBM domains.

As we have demonstrated in this paper, a peripheral effect of high temperature annealing in the presence of DIO is cross-linking in individual pristine films and in the blended film. Knowledge of such reaction may be useful not only in the establishment of fabrication protocols for efficient and long-lasting devices but also in the exploration of patterned deposition techniques.

4. Experimental

All the BHJ layers in this work were prepared on either commercially available indium–tin oxide (ITO) coated glass with layer thickness *ca.* 140 nm and 15 Ω sheet resistances, or on glass microscope slides. Substrates were cleaned using chloroform followed by acetone, Mucasol detergent, and de-ionized water in an ultrasonic bath. The substrates were then washed in a spin-rinse-dryer (SRD) system before being exposed to UV-ozone for 30 min. P3HT (Rieke Metals, M_w 45 k) and PCBM (Nano-C) were dissolved in chlorobenzene and stirred at 60 °C overnight before spin-coating to ensure that the polymer and fullerene have been completely dissolved. BHJ layers were prepared by mixing either 1:4 or 1:1 volume ratio of P3HT to PCBM. 4 vol.% of solvent additives were added where necessary. BHJ layers used for ROM (Nikon Labophot-2), and UV–vis-NIR spectroscopy (Perkin Elmer Lambda 750) were approximately 80 nm thick. Samples for DSC (Mettler Toledo) studies were prepared by first depositing the BHJ solution onto cleaned microscope slides and then delaminating the BHJ layers of interest from the glass substrate and weighing it into an aluminum crucible. Sample weight is between 6 and 8 mg. Aluminum crucibles were sealed with a pierced lid. Heating curves were collected from −100 °C to 300 °C, at a rate of 10 °C min^{-1}, with and without an isothermal step at 150 °C for 30 min prior to heating scans. BHJ layer thickness was controlled by changing both concentration of the casting solution and spinning speed. Sample thickness was determined using a Dektak surface profiler that was calibrated to a Si–SiO_2 ellipsometry standard.

For NMR studies, thin films (*ca.* 80 nm) with 2 vol.% additives were cast on glass. The films were either immediately redissolved in 100 μl D-chloroform (Cambridge Isotopes) or were annealed for 5 min at 150 °C in a nitrogen glovebox and quenched to room temperature before being dissolved in D-chloroform. The dissolved films were subsequently injected into NMR tubes in a nitrogen glovebox. 1H spectra were acquired on a Bruker Avance 600 spectrometer using the zg30 pulse program, signal averaged for 1024 scans.

For device fabrication, the ITO was spin-coated with 40 nm of PEDOT:PSS (Baytron P Al 4083, HC Starck). The PEDOT:PSS coated samples were then heat treated at 110 °C for 3 min and subsequently moved into a nitrogen glove box for the remainder of the device fabrication and measurement. The active layer of the solar cells were spin-coated from a 1:1 mixture of P3HT and PCBM. After spin-coating of the active layer, the samples were moved to a high vacuum chamber (*ca.* 10^{-6} mbar), where an electrode of 150 nm Al were vapor-deposited through a mask resulting in six solar cells with an active area of 0.1690 cm^2. After metal deposition, the samples were measured before and after annealing for 5 min at 150 °C in an N_2 glove box. Samples were then aged at 80 °C under open circuit conditions (i.e. disconnected from load) in a nitrogen glove box, and measured periodically over 330 h. *I–V* curves of the samples were measured using a Keithley 2420 source measurement unit in an N_2 glove box. AM

1.5 illumination at 120 mW cm^{-2} (1.2 SUN) was provided by a solar simulator (Radiant Source Technology). All reported values are not corrected for spectral mismatch.

Acknowledgement

This work is supported by the National Science Foundation Energy for Sustainability Program under Award No. 0933435. L.C. is supported by ConocoPhillips graduate fellowship.

Appendix A. Supplementary material

Supplementary data associated with this article can be found, in the online version, at http://dx.doi.org/10.1016/j.orgel.2013.06.016.

References

[1] G. Yu, J. Gao, J.C. Hummelen, F. Wudl, A.J. Heeger, Polymer photovoltaic cells – enhanced efficiencies via a network of internal donor–acceptor heterojunctions, Science 270 (5243) (1995) 1789–1791.
[2] J.J.M. Halls, C.A. Walsh, N.C. Greenham, E.A. Marseglia, R.H. Friend, S.C. Moratti, A.B. Holmes, Efficient photodiodes from interpenetrating polymer networks, Nature 376 (6540) (1995) 498–500.
[3] K.W. Chou, B. Yan, R. Li, E.Q. Li, K. Zhao, D.H. Anjum, S. Alvarez, R. Gassaway, A. Biocca, S.T. Thoroddsen, A. Hexemer, A. Amassian, Spin-cast bulk heterojunction solar cells: a dynamical investigation, Adv. Mater. 25 (13) (2013) 1923–1929.
[4] F. Padinger, R.S. Rittberger, N.S. Sariciftci, Effects of postproduction treatment on plastic solar cells, Adv. Funct. Mater. 13 (1) (2003) 85–88.
[5] W. Ma, C. Yang, X. Gong, K. Lee, A.J. Heeger, Thermally stable, efficient polymer solar cells with nanoscale control of the interpenetrating network morphology, Adv. Funct. Mater. 15 (2005) 1617–1622.
[6] X. Yang, J. Loos, S.C. Veenstra, W.J.H. Verhees, M.M. Wienk, J.M. Kroon, M.A.J. Michels, R.A.J. Janssen, Nanoscale morphology of high-performance polymer solar cells, Nano Lett. 5 (4) (2005) 579–583.
[7] P. Vanlaeke, A. Swinnen, I. Haeldermans, G. Vanhoyland, T. Aernouts, D. Cheyns, C. Deibel, J. D'Haen, P. Heremans, J. Poortmans, J.V. Manca, P3HT/PCBM bulk heterojunction solar cells: Relation between morphology and electro-optical characteristics, Sol. Energy Mater. Sol. Cells 90 (14) (2006) 2150–2158.
[8] D.E. Markov, E. Amsterdam, P.W.M. Blom, A.B. Sieval, J.C. Hummelen, Accurate measurement of the exciton diffusion length in a conjugated polymer using a heterostructure with a side-chain cross-linked fullerene layer, J. Phys. Chem. A 109 (24) (2005) 5266–5274.
[9] X. Yang, J.K.J. van Duren, R.A.J. Janssen, M.A.J. Michels, J. Loos, Morphology and thermal stability of the active layer in poly(p-phenylenevinylene)/methanofullerene plastic photovoltaic devices, Macromolecules 37 (6) (2004) 2151–2158.
[10] [10] M.O. Reese, S.A. Gevorgyan, M. Jørgensen, E. Bundgaard, S.R. Kurtz, D.S. Ginley, D.C. Olson, M.T. Lloyd, P. Morvillo, E.A. Katz, A. Elschner, O. Haillant, T.R. Currier, V. Shrotriya, M. Hermenau, M. Riede, K.R. Kirov, G. Trimmel, T. Rath, O. Inganäs, F. Zhang, M. Andersson, K. Tvingstedt, M. Lira-Cantu, D. Laird, C. McGuiness, S. Gowrisanker, M. Pannone, M. Xiao, J. Hauch, R. Steim, D.M. DeLongchamp, R. Rösch, H. Hoppe, N. Espinosa, A. Urbina, G. Yaman-Uzunoglu, J.-B. Bonekamp, A.J.J.M. van Breemen, C. Girotto, E. Voroshazi, F.C. Krebs, Consensus stability testing protocols for organic photovoltaic materials and devices, Sol. Energy Mater. Sol. Cells 95 (5) (2011) 1253–1267.
[11] S.E. Shaheen, C.J. Brabec, N.S. Sariciftci, F. Padinger, T. Fromherz, J.C. Hummelen, 2.5% Efficient organic plastic solar cells, Appl. Phys. Lett. 78 (6) (2001) 841–843.
[12] J.K.J. van Duren, X.N. Yang, J. Loos, C.W.T. Bulle-Lieuwma, A.B. Sieval, J.C. Hummelen, R.A.J. Janssen, Relating the morphology of poly(p-phenylene vinylene)/methanofullerene blends to solar-cell performance, Adv. Funct. Mater. 14 (5) (2004) 425–434.
[13] S. Miyanishi, K. Tajima, K. Hashimoto, Morphological stabilization of polymer photovoltaic cells by using cross-linkable poly(3-(5-hexenyl)thiophene), Macromolecules 42 (5) (2009) 1610–1618.
[14] M. Sommer, A. Lang, M. Thelakkat, Crystalline–crystalline donor–acceptor block copolymers, Angew. Chem., Int. Ed. 47 (41) (2008) 7901–7904.
[15] O. Inganäs, F.L. Zhang, M.R. Andersson, Alternating polyfluorenes collect solar light in polymer photovoltaics, Acc. Chem. Res. 42 (11), 1731–1739.
[16] S. Miyanishi, Y. Zhang, K. Tajima, K. Hashimoto, Fullerene attached all-semiconducting diblock copolymers for stable single-component polymer solar cells, Chem. Commun. 46 (36) (2010) 6723–6725.
[17] Y. Kim, S.A. Choulis, J. Nelson, D.D.C. Bradley, S. Cook, J.R. Durrant, Device annealing effect in organic solar cells with blends of regioregular poly(3-hexylthiophene) and soluble fullerene, Appl. Phys. Lett. 86 (6) (2005) 063502.
[18] G. Li, V. Shrotriya, J. Huang, Y. Yao, T. Moriarty, K. Emery, Y. Yang, High-efficiency solution processable polymer photovoltaic cells by self-organization of polymer blends, Nat. Mater. 4 (2005) 864–868.
[19] F.L. Zhang, K.G. Jespersen, C. Björström, M. Svensson, M.R. Andersson, V. Sundströam, K. Magnusson, E. Moons, A. Yartsev, O. Inganäs, Influence of solvent mixing on the morphology and performance of solar cells based on polyfluorene copolymer/fullerene blends, Adv. Funct. Mater. 16 (5) (2006) 667–674.
[20] J. Peet, C. Soci, R.C. Coffin, T.Q. Nguyen, A. Mikhailovsky, D. Moses, G.C. Bazan, Method for increasing the photoconductive response in conjugated polymer/fullerene composites, Appl. Phys. Lett. 89 (25) (2006) 252105.
[21] A.J. Moulé, K. Meerholz, Controlling morphology in polymer–fullerene mixtures, Adv. Mater. 20 (2) (2008) 240–245.
[22] J.K. Lee, W.L. Ma, C.J. Brabec, J. Yuen, J.S. Moon, J.Y. Kim, K. Lee, G.C. Bazan, A.J. Heeger, Processing additives for improved efficiency from bulk heterojunction solar cells, J. Am. Chem. Soc. 130 (11) (2008) 3619–3623.
[23] F.C. Chen, H.C. Tseng, C.J. Ko, Solvent mixtures for improving device efficiency of polymer photovoltaic devices, Appl. Phys. Lett. 92 (10) (2008) 103316.
[24] D. Chirvase, J. Parisi, J.C. Hummelen, V. Dyakonov, Influence of nanomorphology on the photovoltaic action of polymer–fullerene composites, Nanotechnology 15 (9) (2004) 1317–1323.
[25] W.H. Baek, H. Yang, T.S. Yoon, C.J. Kang, H.H. Lee, Y.S. Kim, Effect of P3HT:PCBM concentration in solvent on performances of organic solar cells, Sol. Energy Mater. Sol. Cells 93 (8) (2009) 1263–1267.
[26] M.T. Dang, G. Wantz, H. Bejbouji, M. Urien, O.J. Dautel, L. Vignau, L. Hirsch, Polymeric solar cells based on P3HT:PCBM: role of the casting solvent, Sol. Energy Mater. Sol. Cells 95 (12) (2011) 3408–3418.
[27] H. Hoppe, N.S. Sariciftci, Morphology of polymer/fullerene bulk heterojunction solar cells, J. Mater. Chem. 16 (1) (2006) 45–61.
[28] [28] Y. Yao, J.H. Hou, Z. Xu, G. Li, Y. Yang, Effect of solvent mixture on the nanoscale phase separation in polymer solar cells, Adv. Funct. Mater. 18 (12) (2008) 1783–1789.
[29] N.D. Treat, M.A. Brady, G. Smith, M.F. Toney, E.J. Kramer, C.J. Hawker, M.L. Chabinyc, Interdiffusion of PCBM and P3HT reveals miscibility in a photovoltaically active blend, Adv. Energy Mater. 1 (1) (2011) 82–89.
[30] D.R. Kozub, K. Vakhshouri, L.M. Orme, C. Wang, A. Hexemer, E.D. Gomez, Polymer crystallization of partially miscible polythiophene/fullerene mixtures controls morphology, Macromolecules 44 (14) (2011) 5722–5726.
[31] B.A. Collins, J.R. Tumbleston, H. Ade, Miscibility, crystallinity, and phase development in P3HT/PCBM solar cells: toward an enlightened understanding of device morphology and stability, J. Phys. Chem. Lett. 2 (24) (2011) 3135–3145.
[32] J.D. Roehling, K.J. Batenburg, F.B. Swain, A.J. Moulé, I. Arslan, Three-dimensional concentration mapping of organic blends, Adv. Funct. Mater. 23 (17) (2012) 2115–2122.
[33] H.W. Ro, B. Akgun, B.T. OConnor, M. Hammond, R.J. Kline, C.R. Snyder, S.K. Satija, A.L. Ayzner, M.F. Toney, C.L. Soles, D.M. DeLongchamp, Poly(3-hexylthiophene) and [6,6]-phenyl-c61-butyric acid methyl ester mixing in organic solar cells, Macromolecules 45 (16) (2012) 6587–6599.
[34] [34] A.J. Moulé, K. Meerholz, Morphology control in solution-processed bulk-heterojunction solar cell mixtures, Adv. Funct. Mater. 19 (19) (2009) 3028–3036.
[35] H.Y. Chen, H. Yang, G. Yang, S. Sista, R. Zadoyan, G. Li, Y. Yang, Fast-grown interpenetrating network in poly(3-hexylthiophene): methanofullerenes solar cells processed with additive, J. Phys. Chem. C 113 (18) (2009) 7946–7953.

[36] L. Chang, H.W.A. Lademann, J.-B. Bonekamp, K. Meerholz, A.J. Moulé, Effect of trace solvent on the morphology of P3HT:PCBM bulk heterojunction solar cells, Adv. Funct. Mater. 21 (10) (2011) 1779–1787.
[37] [37] S. Bistac, J. Schultz, Solvent retention in solution-cast films of PMMA: study by dielectric spectroscopy, Prog. Org. Coat. 31 (4) (1997) 347–350.
[38] J. García-Turiel, B. Jérôme, Solvent retention in thin polymer films studied by gas chromatography, Colloid Polym. Sci. 285 (14) (2007) 1617–1623.
[39] J.C. Bijleveld, V.S. Gevaerts, D. Di Nuzzo, M. Turbiez, S.G.J. Mathijssen, D.M. de Leeuw, M.M. Wienk, R.A.J. Janssen, Efficient solar cells based on an easily accessible diketopyrrolopyrrole polymer, Adv. Mater. 22 (35) (2010) E242–E246.
[40] B.R. Aïch, J. Lu, S. Beaupré, M. Leclerc, Y. Tao, Control of the active layer nanomorphology by using co-additives towards high-performance bulk heterojunction solar cells, Org. Electron. 13 (9) (2012) 1736–1741.
[41] [41] J.W. Kiel, B.J. Kirby, C.F. Majkrzak, B.B. Maranville, M.E. Mackay, Nanoparticle concentration profile in polymer-based solar cells, Soft Matter 6 (3) (2010) 641–646.
[42] S.A. Mauger, L. Chang, S. Friedrich, C.W. Rochester, D.M. Huang, P. Wang, A.J. Moulé, Self-assembly of selective interfaces in organic photovoltaics, Adv. Funct. Mater. (2012), http://dx.doi.org/10.1002/adfm.201201874.
[43] M. Campoy-Quiles, T. Ferenczi, T. Agostinelli, P.G. Etchegoin, Y. Kim, T.D. Anthopoulos, P.N. Stavrinou, D.D.C. Bradley, J. Nelson, Morphology evolution via self-organization and lateral and vertical diffusion in polymer: fullerene solar cell blends, Nat. Mater. 7 (2) (2008) 158–164.
[44] [44] Z.Y. Wu, A. Petzold, T. Henze, T. Thurn-Albrecht, R.H. Lohwasser, M. Sommer, M. Thelakkat, Temperature and molecular weight dependent hierarchical equilibrium structures in semiconducting poly(3-hexylthiophene), Macromolecules 43 (10) (2010) 4646–4653.
[45] A.C. Mayer, M.F. Toney, S.R. Scully, J. Rivnay, C.J. Brabec, M. Scharber, M. Koppe, M. Heeney, I. McCulloch, M.D. McGehee, Bimolecular crystals of fullerenes in conjugated polymers and the implications of molecular mixing for solar cells, Adv. Funct. Mater. 19 (8) (2009) 1173–1179. mayer, A.C. Toney, Michael F. Scully, Shawn R. Rivnay, Jonathan Brabec, Christoph J. Scharber, Marcus Koppe, Marcus Heeney, Martin McCulloch, Iain McGehee, Michael D.
[46] B.A. Collins, E. Gann, L. Guignard, X. He, C.R. McNeill, H. Ade, Molecular miscibility of polymer–fullerene blends, J. Phys. Chem. Lett. 1 (21) (2010) 3160–3166.
[47] J. Zhao, A. Swinnen, G. Van Assche, J. Manca, D. Vanderzande, B.V. Mele, Phase diagram of P3HT/PCBM blends and its implication for the stability of morphology, J. Phys. Chem. B 113 (6) (2009) 1587–1591.
[48] D. Chen, A. Nakahara, D. Wei, D. Nordlund, T.P. Russell, P3HT/PCBM bulk heterojunction organic photovoltaics: correlating efficiency and morphology, Nano Lett. 11 (2) (2011) 561–567.
[49] F.C. Jamieson, E.B. Domingo, T. McCarthy-Ward, M. Heeney, N. Stingelin, J.R. Durrant, Fullerene crystallisation as a key driver of charge separation in polymer/fullerene bulk heterojunction solar cells, Chem. Sci. 3 (2) (2012) 485–492.
[50] H.Y. Chen, J.H. Hou, S.Q. Zhang, Y.Y. Liang, G.W. Yang, Y. Yang, L.P. Yu, Y. Wu, G. Li, Polymer solar cells with enhanced open-circuit voltage and efficiency, Nat. Photonics 3 (11) (2009) 649–653.
[51] C. Müller, T.A.M. Ferenczi, M. Campoy-Quiles, J.M. Frost, D.D.C. Bradley, P. Smith, N. Stingelin-Stutzmann, J. Nelson, Binary organic photovoltaic blends: a simple rationale for optimum compositions, Adv. Mater. 20 (18) (2008) 3510–3515.
[52] S.D. Royce, G.D. Figuly, N.P. Khasat, J.R. Matos, Crosslinked polymeric ammonium salts, US Patent 5556619, issued September 17, 1996.